Flash combustion synthesis using two different fuels and characterization of LiF-doped TiO2 for the photocatalytic applications

Israa Zahwa, Mohamed Mouyane, Ahmad Kassas, Alexis Ngueteu Kamlo, Cherif Moslah, Javier Navas, Stefano Livraghi, Jérôme Bernard, Jaafar El Falah, Joumana Toufaily, et al.

Flash combustion synthesis using two different fuels and characterization of LiF-doped TiO_2 for the photocatalytic applications

Israa Zahwa [a,b*], Mohamed Mouyane [a], Ahmad Kassas [b,d], Alexis Ngueteu Kamlo [a,h], Cherif Moslah [a], Javier Navas [f], Stefano Livraghi [g], Jérôme Bernard [a], Jaafar El Falah [c], Joumana Toufaily [b], Tayssir Hamieh [b,e] and David Houivet [a].

[a] Laboratoire Universitaire des Sciences Appliquées de Cherbourg (LUSAC), ER 4253, Université de Caen - Normandie, BP 78, 50130 Cherbourg-en-Cotentin, France.

[b] Laboratoire de Matériaux, Catalyse, Environnement et Méthodes analytiques (MCEMA), EDST, Université Libanaise, Campus Rafic Hariri, Hadath, Beyrouth, Liban .

[c] Laboratoire de Catalyse et de Spectrochimie, Ecole Nationale d'Ingénieurs de Caen, Université de Caen Normandie, Caen, France .

[d] International University of Beirut, School of Engineering, Department of Industrial Engineering, Beirut, Lebanon.

[e] Faculty of Science and Engineering, Maastricht University, P.O. Box 616, 6200 MD Maastricht, Netherlands.

[f] Departamento de Química Física, Facultad de Ciencias, Universidad de Cádiz, E-11510 Puerto Real (Cádiz), Spain.

[g] Dipartimento di Chimica and NIS, Universita ` di Torino, Via P. Giuria 7, 10125 Torino, Italy.

[h] BP 47 ENS, Université Yaoundé 1, Cameroun.

[*] Corresponding author. Email address: israa.zahwa@etu.unicaen.fr (I. Zahwa).

Present address: LUSAC laboratory, 60, rue Max-Pol Fouchet 50130 Cherbourg- en-Cotentin, France (I. Zahwa).

Abstract

The flash combustion method was used to prepare LiF-doped TiO_2 photocatalysts materials using glycine or urea as a fuel with different weight percentage of LiF. The synthesized powders have been characterized by thermal gravimetric analysis (TGA), scanning electron microscopy (SEM) with energy dispersive spectrometer (EDX) analyzer, the specific surface area measurement was performed by BET. The crystallization and the phase transformation anatase-rutile for the powders have been verified by XRD. SEM micrographs for these powders shows the presence of nanoparticles. To investigate the optical band gap of the synthesized samples, UV-Vis spectroscopy was conducted using the diffuse reflectance mode (DRS). The O^{2-}/F^{-} substitution and the presence of Ti^{3+} centers was confirmed by electron paramagnetic resonance (EPR) analysis. The photocatalytic activity of the TiO_2-*x*LiF powders were evaluated through the photocatalytic degradation of Methylene blue (MB) in water under UV-visible light exposure. The results indicated that during the flash combustion synthesis, the nature of the fuel and the percentage of the doping element led to the presence of different polymorphs of TiO_2 which influences the photocatalytic efficiency attributed to the synergistic effect between the two phases (anatase and rutile). The LiF-doped TiO_2 powders synthesized by flash combustion in both cases (by using glycine or urea) showed high performance in MB degradation compared to commercial TiO_2 and undoped synthesized TiO_2 powders, with an optimal degradation of 99 % achieved with 2 wt. % LiF-doped TiO_2 using glycine as a fuel and after 6 hours of UV-Vis irradiation.

Keywords: Flash combustion synthesis; fuels; TiO_2-LiF; nanoparticles; photocatalytic activity.

1. Introduction

Titanium dioxide (TiO_2) is widely used in energy and environmental technologies, particularly as a photocatalyst in air and water purification systems and in water splitting under visible light irradiation [1],[2]. Its high chemical stability, availability, environmental friendliness, non-corrosiveness, and low cost make it an attractive semi-conductor [3],[4]. However, its applications in photocatalysis are limited by its large band gap of 3.2 eV, which only allows for ultraviolet light absorption, only 5% of the solar spectrum [5]. Additionally, the rapid recombination of charge carriers decreases its photocatalytic efficiency [6]. To overcome these limitations, TiO_2 can be modified by doping with metals [7] and non-metals [8], or coupling with other semiconductors [9],[10], to improve its absorption in the visible range and reduce the recombination of photogenerated charges. Doping TiO_2 with non-metallic elements, such as Boron, Carbon, Nitrogen, Phosphorus, Sulfur, and Fluorine, has been shown to improve its photocatalytic activity [11],[12]. Fluorine doping is particularly interesting as it is both a non-metal and a halogen group member [13],[14],[15].

According to Yu *et al*. [16], Fluorine doping leads to the formation of Ti^{3+} cation by balancing the charge between Ti^{4+} cation and F^- anion, which reduces the recombination of photogenerated pairs and enhances the photocatalytic activity. Li *et al*. [17] confirmed that F-doping in TiO_2 increases its photocatalytic activity under visible light through the creation of oxygen vacancies. On the other hand, the presence of metals in the TiO_2 network has a significant impact on its photocatalytic activity [18]. Lithium doping results in a substantial increase in OH radicals on the surface of TiO_2, thus improving its photocatalytic activity [19]. In 2008, Jiang *et al*. synthesized LiF-doped TiO_2 through the sol gel method and demonstrated that it exhibited improved photocatalytic activity compared to undoped TiO_2 [20]. To our knowledge, this is the only paper published on LiF-doped TiO_2 for the photocatalytic applications.

Various synthesis methods have been used for the preparation of TiO_2. The predominant approaches employed in the production of oxide nanomaterials involve liquid phase techniques, such as sol–gel method, precipitation/coprecipitation method, microemulsion method, sonochemical method, hydrothermal/solvothermal method, microwave synthesis, electrochemical synthesis, and template-assisted electrochemical synthesis [21]. These methods offer several advantages including the ability to operate at low temperatures, achieve homogeneous mixing of precursors at the molecular level, and tailor the physical-chemical properties of the resulting oxide nanomaterials (such as particle size, shapes and surface properties), based on the choice of precursors. However, drawbacks exist, like the necessity for costly precursors and extended synthesis durations [22].

Among these methods, combustion synthesis has been reported as a highly efficient methodology conductive to the synthesis and development of diverse materials including oxides [23], it serves as an

efficient methodology that conserves both time and energy resources [24]. This technique is based on an exothermic redox reaction between a metal precursor, typically in the form of nitrate (serving as an oxidizer), and an organic compound (serving as a reductor) in a solvent (typically water) [25], [26]. The flash combustion process is widely used to prepare inorganic ceramic and composite materials with controlled properties for various applications, ranging from catalysis to photocatalysis and electrocatalysis, etc... [27], [28], [29]. The final products obtained through this method possess high reactivity, purity, homogeneity, fine particle size, and high specific surface area [30],[31]. The combination between a large specific surface area and fine particles, characteristic of materials obtained by F.C., could be enhance the photocatalytic efficiency.

In this study, we have synthesized the powders using two different fuels, glycine ($C_2H_5NO_2$) and urea ($CO(NH_2)_2$), in order to compare the effect of the fuel on the synthesis progress and the properties of the powders produced in each case. The type of fuels can play a crucial role in the F.C. reaction. Fuels differ in their reducing power, combustion temperature, and the amount of gas they generate, which affects the properties of the final product in each case [32], [33].

As a dopant material, we have chosen lithium fluoride (LiF) in this work, and our research revolves around the examination of how varying concentrations of LiF dopant and the choice of fuel sources (glycine or urea) affect the crystalline phases, microstructural characteristics, and consequently the photocatalytic performance of titanium dioxide (TiO_2) doped with LiF.

2. Experimental section

2.1 Synthesis of LiF-TiO_2 powders

The reagents used in this synthesis process are the following: glycine ($C_2H_5NO_2$, Sigma ALDRICH, reagent grade ≥ 99%) or urea ($CO(NH_2)_2$, Sigma ALDRICH, reagent grade ≥ 99%) that acted as reducers, nitric acid (HNO_3, Chimix, 67% reagent grade), lithium fluoride (LiF, Alfa Aesar, 98.5% reagent grade) and Titanium IV Butoxide ($Ti(C_4H_9O)_4$, Sigma ALDRICH, 97% reagent grade). Deionized water was used throughout the process. In the flash combustion method, the precursors of nitrate salts are preferred, because they serve as water-soluble low temperature nitrogen source for the synthesis [34]. Here, the preparation of the nitrate precursor ($TiO(NO_3)_2$) was made according to the synthesis method described in the work of Yin *et al*. [35] as a first step. Then, the dopant agent (LiF) and the fuel were added to the solution in order to produce a gel. The combustion of the gel was realized in a tubular furnace under air. In these two paragraphs, we will detail the two synthesis stages.

2.1.1 Synthesis of $TiO(NO_3)_2$

This process consists of forming the nitrate precursor $TiO(NO_3)_2$ which acted as an oxidizer. In the first step, titanium oxo-hydroxide ($TiO(OH)_2$) was formed through the hydrolysis of titanium butoxide ($Ti(C_4H_9O)_4$) by mixing the butoxide with deionized water and stirring for five minutes **(Eq. 1)**. The resulting precipitate was filtered and washed with deionized water three times to remove any butanol

traces. In the second step, the titanium hydroxide precipitate was dissolved in nitric acid (HNO_3) under stirring for ten minutes in order to form the nitrate precursor $TiO(NO_3)_2$ **(Eq. 2)**.

$$Ti(OC_4H_9)_4 + 3H_2O \rightarrow TiO(OH)_2 + 4C_4H_9OH \quad \textbf{(Eq. 1)}$$

$$TiO(OH)_2 + 2HNO_3 \rightarrow TiO(NO_3)_2 + 2H_2O \quad \textbf{(Eq. 2)}$$

2.1.2 Synthesis of TiO_2-xLiF

Once $TiO(NO_3)_2$ has been prepared, appropriate quantities of LiF and glycine ($C_2H_5NO_2$) or urea ($CO(NH_2)_2$) are added to the solution formed under stirring at 120 °C in order to concentrate the resulting solution. The combustion temperature is influenced by the value of φ that is determined by using the valence of the oxidizers elements and that of the reducers, this value influences the reactivity of the synthesized powder and its structural and microstructural properties. Previous studies have shown that the optimal conditions for combustion were observed for φ=1 [36]. So, in our case, we calculate the stoichiometry of the fuel with a value of φ equal to 1. The "Oxidizers/Reducers" ratio noted φ= O/F is used to calculate the stoichiometry of the fuel based on the following balanced reactions **(Eq. 3 and 4)**:

With glycine:

$$9TiO(NO_3)_2 + 10C_2H_5NO_2 + (x\ LiF) \rightarrow 9TiO_2 + (xLiF) + 25H_2O + 20CO_2 + 14N_2 \quad \textbf{(Eq.3)}$$

With urea:

$$3TiO(NO_3)_2 + 5CO(NH_2)_2 + (x\ LiF) \rightarrow 3TiO_2 + (xLiF) + 10H_2O + 5CO_2 + 8N_2 \quad \textbf{(Eq. 4)}$$

Noting that the doping agent (LiF) is not involved in the chemical reactions and is considered as a spectator species.

These reactions show that gas content produced in each case with the two fuels are not the same. After adding LiF and fuel, the gel formed is transferred to an alumina crucible in a stainless-steel box and introduced into a furnace for combustion, this furnace is heated under air with a ramp about 450 K/h, and then switched off when the exothermic reaction is occurred. Furthermore, the actual temperature closest to the powders was monitored using a thermocouple positioned at the crucible level, situated within the metallic container placed inside the furnace. This temperature consistently remained below 400 °C, except during the brief and intense flash peak. Following this phase, an exothermic reaction becomes evident within a few minutes.

Subsequently, the combustion product was delicately pulverized into a powder form using an agate mortar, resulting in the formation of yellowish-white powders. Lastly, these acquired materials underwent a heat treatment at 500 °C for a duration of one hour in an atmospheric condition, in accordance with the subsequently presented results of thermogravimetric analysis. This process was carried out to eliminate any unreacted organic residues from the flash synthesis, enhance the crystalline

structure of the powders, and facilitate the formation of the desired phase incorporating the doping element (LiF).

In order to investigate the impact of LiF doping on the phase composition and photocatalytic performance of TiO_2 powders, different compositions have been synthesized denoted as TiO_2-*x*LiF, where *x* represents the weight percentage (wt.%) of LiF (*x*= 0.25, 0.5, 0.75, 1, 2 and 5). Furthermore, an undoped TiO_2 sample (*x*= 0) was synthesized using the same procedure to serve as a reference point for comparison. Fig. 1 summarizes the different sequential stages involved in the synthesis of TiO_2-*x*LiF powders via the flash combustion method.

2.2 Characterization

The phases and crystalline structures of the materials were characterized by X-ray diffraction used the diffractometer Inel Equinox 3000 equipped with a copper anticathode tube. Thermogravimetric analysis (TGA) was conducted in a Setaram TG-DTA92 using an alumina crucible between Room Temperature and 900 °C with a heating rate of 5 °C/min under air.

The microstructural of the powders were investigated using high-resolution scanning electron microscope (SEM) equipped with energy dispersive spectrometer (EDX) analyzer. The specific surface area and pore size distribution of samples were determined by the gas adsorption method according to the theory of Brunauer, Emmett and Teller BET (method of 5 points) and BJH (method of 80 points) respectively. The analyzer used is a Tristar II from Micromeritics brand. UV-Vis spectroscopy in the diffuse reflectance mode was performed to study the optical band gap of the samples. The spectra were collected by using a system assembled in our laboratory composed of an integrating sphere supplied by Spectra Tech, a USB2000 + spectrometer from Ocean Optics, and a Xe lamp, model ASB-XE-175, supplied by Spectral Products.

Continuous Wave Electron Paramagnetic Resonance (CW-EPR) experiments were performed with a Bruker EMX spectrometer operating at X-band (9.5 GHz), equipped with a cylindrical cavity operating at 100 kHz field modulation. All the spectra were recorded in vacuum condition at 77 K in a EPR cell that can be connected to a conventional high-vacuum apparatus (residual pressure < 10^{-4} mbar). In all cases the parameters setup were Modulation Amplitude 0.2 mT and microwave power of 1 mW. The EPR spectra of the powders upon irradiation and in vacuum condition were recorded in the EPR cavity illuminated by a 500 W Newport Hg-Xe lamp.

2.3 Photocatalytic activity measurement

The photocatalytic activities of LiF-TiO_2 powders were evaluated by the decomposition of methylene blue (MB) in water. For the photodegradation test, in a typical experiment 0.2g of powder as prepared and after heat treatment was introduced into a solution of MB of C= 5.92 mg/L. The solution with the powders were transferred to a double jacketed reactor with cooling water and placed in a black

box in order to block the entrance of any external light. Then, the mixture was stirred in the dark for 30 min to establish an adsorption/desorption equilibrium between the photocatalyst and the MB molecules.

The distance between the liquid surface and the illumination source was fixed at 30 cm, a 400 W halogen lamp (UV-Visible) was used as a light source and the light intensity measured at the reactor surface was approximately 7000 lux. Samples were collected from the irradiated solution at predetermined time intervals. Once the irradiation terminated, the samples were centrifuged for 10 min for removal of the catalyst. Photodegradation was determined by measuring the absorbance at λ_{max}= 664 nm (MB) on a UV-Vis spectrophotometer (SECOMAM-UViLine 9600). The conversion rate ($\%\tau$) of MB which represents the ratio between the quantity of reactant transformed and the initial quantity was calculated according to the equation 5, where C_0 and C_t (mg/L) are the initial and the concentration of MB at time t respectively:

$$\%\tau = \left({C_0 - C_t}/{C_0}\right) \cdot 100 \qquad \textbf{(Eq.5)}$$

3. Results and discussion

3.1 Monitoring the combustion temperature as a function of time

The temperature as a function of time for all samples with both fuels (glycine and urea) is monitored and depicted in Fig. 2. When employing glycine (Fig. 2a), an exothermic phenomenon is observed characterized by an increase in temperature, starting at approximately 280 °C (as indicated in Table 1, displaying the maximum peak temperature measured by the thermocouple during synthesis).

The highest maximum peak temperature recorded in the synthesis of samples containing 0.25%, 0.75%, and 5% by weight of LiF (Table 1), which results in a pronounced exothermic peak (Fig. 2a) Conversely, samples containing 0% and 0.5% by weight of LiF (as depicted in Fig. 2a) present a small peak or nearly absent. These variations in maximum peak temperature and exothermic peak intensity among the different syntheses with different proportions of LiF can be attributed to distinctions in the hydration rate of the gel preceding the flash reaction and provides insights into the progress of the flash synthesis. Moreover, urea-based samples (Fig. 2b) show more pronounced exothermic phenomena compared with synthesis using glycine, starting at around 100 and rising to 450 °C (Table 2). It is important to note that detecting the exact combustion temperature during all syntheses was not achievable due to the relatively sluggish response time of the thermocouple.

Comparing the effect of using the two different fuels, it is noteworthy that in the case of the synthesis with urea, the maximum peak temperature measured by the thermocouple is higher than that in the synthesis with glycine (Table 1 and Table 2). This difference can be attributed to the distinct chemical compositions, amino acid structures of glycine and urea and from the complexation of the gel formed in the case with each fuel, which in turn influence their respective combustion properties.

3.2 Thermogravimetric analysis (TG)

Weight loss of the powder, prepared by flash combustion, as function of heating temperature analyzed by TGA, has been illustrated in Fig. 3. The curves indicate three distinct stages of mass loss. In the first stage, all samples from both synthesis cases (glycine and urea) (Fig. 3a and 3b) exhibit a weight loss up to 120 °C, corresponding to the evaporation of adsorbed water. However, it is worth mentioning that this loss varies due to the ambient humidity of powders, which differs according to the atmospheric condition change at the preparation time. The second stage of weight loss occurs between 120 °C to 500 °C and is attributed to the decomposition of organic residues [37].

Table 1 and Table 2 summarize the weight loss of the powder prepared with glycine and urea, respectively, within this temperature range. In the case of glycine-based powders, two samples without LiF and with 0.5 wt.% of LiF displayed the highest weight loss, that are 3.9% and 3.8% respectively, as shown in Table 1. Meanwhile, in the urea-based powders, the sample containing 5 wt.% LiF exhibited the highest weight loss, approximately 1.3% (Table 2). This difference in weight loss among these samples are closely linked to the progress of the flash synthesis. These observations can be correlated with our previous thermal results detected via the thermocouple during the F.C. reaction. We noted that when the combustion reaction was not well executed, indicated by a less intense exothermic reaction peak, typically when glycine is used (Fig. 2), the loss of mass was more significant. This suggests that in such cases, there were organic products that did not react, and the flash reaction remained incomplete.

The final stage of weight loss, occurring between 700 to 900 °C, can be assigned to the sublimation of LiF. However, this loss was not observed in all samples, only when LiF is in excess and identified by XRD as indicated in Table 1and Table 2.

Table 1: maximum peak temperature, percentage of weight loss of the as-synthesized samples, presence of LiF XRD peaks, phase compositions and BET surface areas of these samples heat treated at 500 °C, with glycine as fuel.

(TiO_2-*x* LiF)	**$T_{peak\ (max)}$ (°C)**	**Weight loss %**		**Presence of LiF XRD peaks**		**Rutile content (%)**		**S_{BET} ($m^2.g^{-1}$)**
		120-500°C	**700-900°C**	**As-synthesized**	**Calcinated at 500 °C**	**As-synthesized**	**Calcinated at 500 °C**	
0	328	3.9	0	NO	NO	0.04	1.2	63.8
0.25	332	2.3	0	NO	NO	9	11.8	38.9
0.5	299	3.8	0	NO	NO	0.3	10.3	29.1
0.75	347	2.5	0	NO	NO	13	22.5	12
1	329	2.9	0.2	YES	NO	2.5	14.5	17.5
2	328	2.4	0.5	YES	YES	0.4	30.6	17.3
5	332	1.7	0.6	YES	YES	5.8	8.3	10.9

Table 2: maximum peak temperature, percentage of weight loss of the as-synthesized samples, presence of LiF XRD peaks, phase compositions and BET surface areas of these samples heat treated at 500 ºC, with urea as fuel.

(TiO_2-*x* LiF)	$T_{peak\ (max)}$ (°C)	Weight loss %		Presence of LiF XRD peaks		Rutile content (%)		S_{BET} ($m^2.g^{-1}$)
		120-500°C	700-900°C	As-synthesized	Calcinated at 500 ºC	As-synthesized	Calcinated at 500 ºC	
0	445	0.2	0	NO	NO	58.8	79	5.8
0.25	345	0.6	0	NO	NO	37.2	73.7	12.3
0.5	351	0.3	0	NO	NO	61.9	95.5	4.9
0.75	358	0.3	0.2	YES	NO	39.7	93.3	5.8
1	363	0.6	0.2	YES	NO	15.8	69.6	13.7
2	375	0.4	0.3	YES	YES	12.1	32.2	15.2
5	387	1.3	0.3	YES	YES	0.21	3.1	16.7

3.3 Structural X-ray diffraction analysis

To investigate the crystalline structures of the powders before and after heat treatment, X-ray diffraction (XRD) analysis was conducted. The XRD diffractograms for the as-synthesized TiO_2-*x*LiF powders obtained through F.C. synthesis (Fig. 4a and 4b), reveal that, in both cases using glycine and urea, the synthesized TiO_2-*x*LiF crystallized into a mixed phase consisting of anatase and rutile. This observation is consistent with the reference patterns JCPDS no. 21-1272 for anatase, JCPDS no. 21-1276 for rutile and JCPDS no. 45–1460 for LiF. The fraction of the rutile phase (F_R) in each sample was determined using the Spurr equation [38] :

$$F_R = \left\{1 + 0.8\left[{I_A(101)}/{I_R(110)}\right]\right\}^{-1} \quad \textbf{(Eq.6)}$$

Where F_R is the amount of rutile in an anatase and rutile mixed-phase, I_A (101) and I_R (110) are the anatase and rutile main peak integral intensities respectively.

The crystallite sizes of the samples were calculated by applying the Debye-Scherrer equation to the corrected half-height width of the characteristic peaks associated to anatase (101) and rutile (110). The Debye-Scherrer formula is expressed as follows:

$$Cs = {K\lambda}/{(\beta cos\theta)} \quad \textbf{(Eq.7)}$$

Where Cs is the crystallite size, λ is the wavelength of the X-ray radiation (λ =0.15406 nm) for CuK α , the value of K is assumed to be 0.89, β represents the corrected line width at half-maximum height and θ is the diffracting angle.

The phase formation of these samples is influenced by various factors, including the nature of the fuel, the dopant content, and the ignition temperature. Furthermore, these influences can vary depending on the specific synthesis conditions employed in each study.

S. Challagulla *et al.* [39] synthesized undoped TiO_2 using F.C. process and observed that TiO_2 crystallized in the anatase phase when glycine was used as the fuel, while a mixed phase was observed when urea was used as the fuel. In our study, we synthesized undoped samples using both glycine and urea as fuels and obtained similar results, confirming the phase outcomes. However, when we introduced LiF as dopant in our samples synthesized with glycine, we observed anatase to rutile phase transformation.

The rutile phase is thermodynamically more stable than the anatase phase and it was mentioned in the literature that the transformation of anatase to rutile is achieved at about 600 °C when calcined in air [40],[41]. However, the anatase-rutile transformation is influenced by the synthesis conditions and it is observed in a temperature range from 400 to 1200 °C, depending on the method of powder synthesis, the amount and type of additive added and the atmosphere [42]. According to this information, the significantly higher rutile content observed in the case of powders synthesized using urea compared to those synthesized using glycine (Table 1 and Table 2) strongly suggests that a higher synthesis temperature was achieved in the former case. This elevated temperature accelerated a substantial phase transformation from anatase to rutile in the urea-synthesized powders.

However, it is important to note that only the sample containing 5wt. % LiF in the glycine-based synthesis contains more rutile than the urea-based counterpart. Nevertheless, based on the results of the thermocouple temperature measurement and the observed weight loss, it appears that this synthesis is incomplete, and the exothermic phenomenon occurs later compared to the other samples (Fig. 2b), which can be delayed the phase transformation in this case. These X-ray diffraction patterns of the as-synthesized TiO_2-*x*LiF powders are consistent with the weight loss curves depicted in Fig. 3a and 3b and the values for weight loss calculated in the temperature range 700-900 °C, where we observe a weight loss in the temperature range 700-900 °C for both sets of samples, the 1, 2 and 5 wt.% LiF using glycine fuel, and the 0.75, 1, 2 and 5 wt.% LiF using urea fuel. Notably, these samples exhibit a characteristic peak corresponding to the LiF phase in the XRD diffractogram at $2\theta=45.2^{o}$ (Table 1 and Table 2).

Fig. 5 depicts X-ray diffraction (XRD) patterns of powdered samples subjected to heat treatment at 500 °C for 1 hour in an air environment. It is evident from the data presented in Table 1 and Table 2 that there is a notable increase in the proportion of the rutile phase following the heat treatment process.

This finding is in agreement with the conclusion drawn by Jiang *et al.* in their study [20], where they confirmed that the introduction of LiF initiates a phase transition from anatase to rutile at a lower temperature. However, it is necessary to note that the extent of this phase change does not exhibit a linear correlation with the LiF concentration increase. This disparity can be attributed to variations in

the subsequent heat treatment and the ignition temperature during the synthesis of the powders which influence the progression of the phase transformation.

The results reveal that, among the tested samples, the glycine-based powder with 2wt. % LiF and the urea-based powder with 0.5wt. % LiF exhibit the most substantial proportion of rutile accounting for 30.6 and 95.5%, respectively.

Furthermore, post-heat treatment analysis reveals the persistence of the LiF phase peak around $2\theta=45.2^{o}$ in the XRD patterns for TiO_2 samples containing 2 wt.% and 5 wt.% LiF, regardless of whether glycine or urea was employed in the synthesis process. This observation can be elucidated by recognizing that the solubility of LiF in the solid is finite. Beyond a certain threshold, the solubility limit of LiF is surpassed, resulting in the enduring presence of the LiF peak in the XRD patterns. These results indicate that the solubility limit of LiF in TiO_2 at 500 °C is around 2% by weight in our case.

Concerning the crystallite size estimated by the Scherrer method in Table 3, we generally measure larger crystallite sizes for the rutile phase than for the anatase phase. These sizes are also slightly higher when using urea compared to glycine related synthesis.

Table 3 : mean crystallite size (Cs) (nm) from XRD of the samples synthesized before and after heat treatment.

(TiO_2-*x* LiF)	**Cs (nm) with glycine**				**Cs (nm) with urea**			
	As- synthesized		**Calcinated at 500 °C**		**As- synthesized**		**Calcinated at 500 °C**	
	anatase	**rutile**	**anatase**	**rutile**	**anatase**	**rutile**	**anatase**	**rutile**
0	9	*	17	31	16	36	21	47
0.25	11	47	21	75	16	36	21	42
0.5	9	*	23	51	18	47	26	51
0.75	13	75	27	49	24	39	29	53
1	9	*	25	68	19	37	29	49
2	12	*	31	53	24	45	30	48
5	17	*	31	*	21	*	33	79

* rutile rate too low for measurement.

3.4 BET specific surface area and pore size distribution analysis

Fig. 6a displays N_2 adsorption-desorption isotherms for TiO_2+2 wt.% LiF samples heat treated at 500 °C, synthesized using either glycine or urea as fuel. These isotherms exhibit a type IV nitrogen isotherm pattern, classified according to IUPAC standards, and feature type H3 desorption hysteresis loops, indicative of capillary condensation within mesoporous structures. Notably, the sample synthesized with glycine exhibited higher adsorption than its urea-synthesized counterpart (as shown in Fig. 6a). Further analysis, as presented in Fig. 6b and 6c, reveals that the powder sample synthesized with glycine as fuel displays mesopores with a pore diameter ranging from 10 to 60 nm, while the

powder sample synthesized with urea as fuel displays mesopores with a diameter ranging from 10 to 75 nm.

The BET specific surface areas of samples subjected to one-hour heat treatment at 500 °C under air are presented in Table 1 and Table 2. Table 1 contains data for samples prepared using glycine, while Table 2 showcases outcomes for samples prepared using urea.

Theoretically, reducing the particle size has the potential to enhance the specific surface area, thereby increasing the number of active sites available on the photocatalyst's surface. This, in turn, mitigates the recombination of electron-hole pairs, ultimately resulting in an improvement in photocatalytic activity [43].

In both cases, where glycine and urea were used, samples with varying percentages of LiF exhibit differences in their specific surface areas. These disparities are influenced by factors such as combustion temperature, post-treatment processes, and the quantity of the dopant. Notably, among the glycine-synthesized powders, the sample lacking LiF exhibits the largest specific surface area at 63.8 m^2/g. It becomes evident that as the percentage of LiF increases in these synthesized powders, the specific surface area decreases. This observation suggests that higher LiF content promotes particle aggregation.

Among the urea-synthesized powders, it is noteworthy that the samples without LiF and those containing 0.75 and 0.5 wt.% LiF exhibit the smallest specific surface areas, measuring 5.8 and 4.9 m^2/g, respectively. In contrast, the sample containing 5 wt.% LiF boasts the largest specific surface area at 16.7 m^2/g. Interestingly, all the samples, except for these three urea-synthesized variants (0, 0.5 and 0.75 wt.% LiF), display a greater specific surface area compared to commercial TiO_2, which has an area of 8.3 m^2/g.

Our findings reveal a correlation between ignition temperature and phase composition. The higher the combustion temperature, the higher the anatase-to-rutile conversion rate and we assume that the specific surface area of the samples is smaller. However, the determination of the specific surface area of powders is conducted exclusively post heat treatment, as pre-treatment measurements are rendered inconsequential. This is attributable to the substantial presence of amorphous carbon and organic residues in powders subsequent to flash synthesis, resulting in an elevated specific surface area in comparison to calcined powders. This abundance of impurities complicates the accurate measurement of the specific surface area and fails to adequately characterize the doped materials (TiO_2-LiF) due to the presence of other substances within these materials.

This observation aligns with the logical explanation that when F.C. synthesis occurs at a higher ignition temperature, the powders are subjected to elevated temperatures, resulting in grain growth and, consequently, reduced specific surface areas.

In a similar way, as the temperature increases, the anatase phase undergoes transformation into rutile. Consequently, in the majority of the synthesized samples, we observe that a higher specific surface area corresponds to anatase being the predominant phase. This dual influence of temperature on both phase transformation and BET specific surface area underscores the intricate relationship between these factors.

3.5 Microstructure and elementary analysis

SEM micrographs displayed in Fig. 7 highlight the substantial influence of the choice of fuel on the morphology of powders during the flash combustion process. Notably, powders synthesized with glycine (Fig. 7a and 7b) exhibit a distinctly different morphology compared to those synthesized with urea (Fig. 7c and 7d).

In the case of glycine-fueled synthesis, the micrograph at low resolution (Fig. 7a) reveals the presence of aggregates measuring approximately 3 μm in size for the larger one. The high-resolution image of this powder (Fig. 7b) shows a spherically particles with the range of 30-90 nm in size.

The TiO_2-*x*LiF powders synthesized with urea (Fig. 7c) presents irregularly shaped aggregates type rock of around 300 μm in size, a morphology reminiscent of the findings by S. Challagulla *et al*. [39], who synthesized TiO_2 via F.C. without the addition of a doping element. These large aggregates are formed of small particles (Fig. 7 d) in the size range of 30-80 nm, consistent approximately with the dimensions observed in the glycine-assisted synthesis. Furthermore, EDX spectra confirm the presence of characteristic peaks of Fluorine, while it is worth noting that our EDX detector does not register Lithium.

3.6 UV-Vis spectroscopy in diffuse reflectance mode

UV-Vis spectroscopy in the diffuse reflectance mode was performed to study the optical band gap of the samples synthesized. From the spectra registered, the optical band-gap energy was determined following the Kubelka– Munk function and the Tauc plot. For diffuse reflectance spectra, the Kubelka–Munk function f (R) is given by:

$$f(R) = \frac{(1-R)^2}{2R} \qquad \textbf{(Eq. 8)}$$

in which *R* is the reflectance. The plot for a semiconductor of $[f(R) \cdot h\nu]^n$ vs $h\nu$ shows a linear region for n=2 and for n=1/2 if the band gap is determined by indirect or direct transition, respectively. For the samples analyzed in this work, a linear region is found for the plot of $[f(R) \cdot h\nu]^n$ vs $h\nu$ when n = ½, satisfying the following equation:

$$[f(R) \cdot h\nu]^{1/2} = K\left(h\nu - E_g\right) \qquad \textbf{(Eq. 9)}$$

Which is known as Tauc plot. In this equation, E_g is the optical band-gap energy, *K* is a specific constant for each semiconductor, and $h\nu$ is the photon energy. Thus, Fig. 8a shows the Tauc plot of samples

synthesized using glycine, and the values of the optical band gap are shown in Table 4. The optical band gap is around of 3 eV for all the samples. The only different behavior is observed for the sample with *x* = 1 wt.%. in which two band gaps are observed. In addition, the values observed in Fig. 8a for low energy, below 3 eV, are similar for all the samples, which means all the samples show similar absorption in the visible range of the electromagnetic spectrum. In addition, Fig. 8b depicts the Tauc plot for the samples synthesized using urea, and Table 4 presents the corresponding optical band gap values. These values approximate 3 eV, although they exhibit a marginal decrease when compared to those of samples synthesized using glycine. Also, notable variations in the values are discerned among the urea-synthesized samples, and the Tauc plot function values are comparatively higher than those shown for the samples synthesized with glycine. This suggests a somewhat greater UV-Visible absorption in the samples prepared using urea.

The variance in the band gap observed between the two synthesis cases (glycine and urea) stems from the differences in the percentage composition of the anatase and rutile phases within the samples, as it reveals the strongest correlation observed in Fig. 9. This figure predominantly demonstrates a decrease in the band gap value for the samples in which rutile was the predominant phase, regardless of the percentage of LiF present. Consequently, samples synthesized with urea exhibit a generally smaller band gap compared to those synthesized using glycine (Table 4), primarily due to the significantly higher rutile phase content in the urea-based samples compared to the glycine-based samples. These results align with those previously reported in the literature that the rutile phase produces larger crystallites (Table 3), thereby potentially leading to a reduction in the band gap energy (Eg) [44].

Moreover, All the synthesized powders using glycine and urea exhibit a band gap value that is nearly lower than the theoretical band gap of both the anatase and rutile phases that are respectively 3.23 and 3.02 eV [45]. This indicates the importance of the LiF dopant, which effectively reduces the band gap of the doped materials (TiO_2-LiF).

Table 4: Optical band gap of the TiO_2+(*x* LiF) samples heat treated at 500 ºC. (Where, *x*=0, 0.25, 0.5, 0.75, 1, 2 and 5).

Glycine		**Urea**	
x	***E_g* / eV**	***x***	***E_g* / eV**
0	3.06±0.01	0	2.84±0.03
0.25	3.03±0.02	0.25	2.91±0.03
0.5	2.94±0.02	0.5	2.78±0.04
0.75	2.95±0.02	0.75	2.83±0.02
1	3.00±0.01	1	2.96±0.03
2	3.01±0.01	2	2.98±0.02
5	3.00±0.02	5	2.99±0.04

3.7 EPR characterization

As elucidated in the introduction section, when fluorine is incorporated into the TiO_2 lattice sites, replacing oxygen atoms lattice, the solid compensates the resulting valence alteration generating an amount of Ti^{3+} ions equivalent to the dopant. This can be expressed by the formula $Ti_{1-x}^{4+}Ti_x^{3+}O_{2-x}^{2-}F_x^-$, which enhances the electron-rich nature (n-character) of the oxide.

To verify this charge compensation, EPR measurement was carried out on TiO_2 sample prepared with 2wt.% LiF using glycine as a fuel (Fig. 10). The EPR results of this sample reveals a complex signal characterized by *g* factors lower than that of a free electron (g_e=2.0023). These results arise from at least two distinct types of Ti^{3+} centers.

In Fig. 10 the center labelled as Ti^{3+}(I) is distinctive to the anatase polymorph and is associated with Ti^{3+} centers occupying regular lattice positions, producing a signal with $g_{//}$ = 1.960 and $g_{\perp}$ =1.991 [46]. This center partially overlaps with a boarder signal denoted as Ti^{3+}(II). In the region were Ti^{3+}(II) is observed, signals amenable to both the anatase and rutile polymorphs are expected. The component at g= 1.977 can be attributed to interstitial Ti^{3+} ions in rutile phase [47]. However, due to the considerable broadening of the line shape, the presence of a second species linked to anatase cannot be excluded [48].

Precise identification of the signal at g = 2.003 poses a challenge, as such a signal is commonly observed in the presence of carbon impurities. However, it is also consistently detected in reduced TiO_2, where it is typically associated with conduction band electrons [49]. Regardless of the origin of this particular spectral feature, the EPR analysis reinforces the evidence of fluorine incorporation into the lattice of both polymorphs comprising the TiO_2 material, affirming the associated charge compensation phenomenon.

Furthermore, the sample was subjected to irradiation with UV-vis light, distinct features at g = 2.018 and g = 2.027 emerged. These features are attributed to trapped holes [50], providing clear confirmation of the photogeneration of oxidizing centers involved in the photo degradation of pollutants.

4. Photocatalytic activities

The assessment of photocatalytic performance in the synthesized materials involved a comparative analysis with commercial TiO_2 in the degradation of Methylene Blue (MB) within an aqueous medium. Following an extensive experimental inquiry, the findings consistently revealed that the materials doped with 2 wt.% LiF, prepared using both glycine and urea, exhibited the highest photocatalytic activity when compared with other samples containing varying proportions of LiF doping.

The photocatalytic performance of these two most promising samples, namely TiO_2 doped with 2 wt.% LiF prepared using glycine and urea, was evaluated and compared against commercial TiO_2 and undoped TiO_2 synthesized through the F.C. method. Fig. 11 a illustrates the degradation of MB as a function of irradiation time for these samples.

To discern the kinetics of photodegradation, experimental data were fitted to the pseudo-first-order reaction model which is given by the following equation:

$$-\ln\left({C_t}/{C_0}\right) = K_{app}\,.\,t \qquad \textbf{(Eq. 10)}$$

Where C_0 and C_t (mg/L) are the initial and the concentration of MB at time t respectively, K_{app} is the apparent rate constant of the first-order reaction (min^{-1}). A plot representing (Eq. 10) is depicted in Fig. 11 b, displaying a straight line, where the slope corresponds to the observed first-order rate constant, denoted as k_{app} and we also calculated the half-reaction times ($t_{1/2}$). The resulting values are summarized in Table 5.

Table 5: Phase compositions, BET surface areas and photocatalytic activity of commercial TiO_2 and the photocatalysts TiO_2 _ *x* LiF.

***x* of photocatalyst**	**Rutile content (%)**	**S_{BET} ($m^2.g^{-1}$)**	**D% (after 360 min)**	**$K_{app} \times 10^{-4}$ (min^{-1})**	**$t_{1/2}$ (min)**	**R^2**
0_urea	79	5.8	62	27	257	0.997
Commercial TiO_2	0	8.3	81	42	165	0.985
0_ glycine	1.2	63.8	82	48	144	0.998
2_urea	32.2	15.2	93	69	100	0.974
2_ glycine	30.6	17.3	99	108	64	0.992

Notably, all the synthesized samples exhibited a higher degradation percentage compared to commercial TiO_2 after 360 min of irradiation, except for the undoped sample synthesized with urea as fuel. In this particular case, the substantial rutile content (79%) and a significantly reduced specific surface area (5.85 m^2g^{-1}) can be attributed to this outcome. This observation underscores that a higher proportion of anatase in the biphasic system tends to enhance photocatalytic efficiency, aligning with existing literature [51], and the study conducted by R.J. Tayade *et al.* [52], which confirmed that the photocatalytic activity of anatase nanocrystalline TiO_2 is higher than that of the rutile phase.

The most substantial MB degradation rate (99%) was attained with powders doped with 2 wt.% LiF prepared using glycine as a fuel. The kinetic analysis further revealed that this sample exhibited the swiftest reaction kinetics (K_{app}=0.0108 min^{-1}, $t_{1/2}$ = 64 min), which is approximately 2.5 times faster than commercial TiO_2. This sample also possessed a specific surface area of 17.3 m^2g^{-1}, a rutile content of 30.6%, and a bandgap energy of 3.01 eV.

However, the sample prepared with glycine and urea do not show significant differences in the bandgap, indicating that this feature alone does not singularly dictate the photocatalytic properties. Additionally, the introduction of F-doping into TiO_2 resulted in the formation of Ti^{3+} ions [53], which were confirmed by EPR analysis in the sample TiO_2 with 2 wt. %LiF prepared with glycine. These Ti^{3+}

ions enhance the *n* character of this oxide and make the electrons more available for the electron transfer at the surface.

As reported by several authors in fact, the introduction of fluorine in the TiO_2 lattice improves the photocatalytic performance under UV light illumination [54]. A further possible contribution to the observed catalytic activity can be due to fluorine ions stabilized at the surface (surface fluorination) that usually accompanies the lattice doping. In this case the fluorine ions substitute the isoelectronic surface hydroxyl groups with no alteration of the charge balance and therefore without generating Ti^{3+} centers. It is well known that surface fluorination has some influence in promoting the photocatalytic activity under ultraviolet irradiation [55]. For this reason, a role of this second type of fluoride ions in the photocatalytic activity of the materials here described cannot be discarded even though it is reasonably lower than that of the bulk ions.

The photocatalytic results underscore the multifaceted nature of the influencing parameters. Specifically, they demonstrate that the variation in the proportion of the anatase-rutile phase has a pronounced impact on MB photodegradation, surpassing the influence of the band gap and the BET-specific surface area. The composite phase improves the catalytic efficiency by exhibiting a synergistic effects in terms of exposed surfaces and electronic structures [56]. The most favorable proportion, leading to superior photocatalytic activity, was found in the polymorph TiO_2+2 wt.% LiF prepared with glycine as a fuel, where the composition consisted of 70% anatase. Furthermore, the introduction of the doping element promoted phase transformation and improved the photocatalytic activity.

5. Conclusions

To summarize, the synthesis of TiO_2-*x*LiF powders via the flash combustion method has been successfully achieved. XRD analysis confirmed the presence of a biphasic structure consisting of anatase and rutile phases, the proportions of which are influenced by the synthesis conditions and the presence of the LiF doping element, promoting phase transformation at relatively low temperatures.

The BET specific surface area measurements revealed variations among the samples, attributable to factors such as ignition temperature, post-treatment, and doping content. SEM micrographs displayed nanoparticles, and EDX analysis confirmed the presence of fluorine in the samples.

Analysis of the bandgap through Diffuse Reflectance Spectroscopy (DRS) showed slight fluctuations among the samples. EPR characterization provided evidence of Ti^{3+} centers in the sample exhibiting the highest photocatalytic activity.

Significantly, the choice of fuel in the flash combustion synthesis influenced the physicochemical properties of the synthesized materials. The sample doped with 2wt.% LiF and prepared with glycine as a fuel displayed exceptional photocatalytic performance, with a remarkably high degradation rate (99%) achieved after 6 hours of irradiation. This performance surpassed that of commercial TiO_2, indicating the superior photocatalytic potential of these LiF-doped powders synthesized via flash combustion.

In our investigation, the enhancement in photocatalytic activity was attributed to the presence of a mixed anatase/rutile phase, with a substantial proportion of anatase (70% in our case). The synergistic interactions between these two phases mitigated photogenerated pair recombination, resulting in improved photocatalytic efficiency and we have clearly demonstrated that in this work in comparison with the commercial TiO_2, which is composed of a single phase "anatase".

These outcomes suggest that LiF-doped TiO_2 powders exhibits promising potential as a suitable candidate for the photocatalytic degradation of organic contaminants in water, and may also hold promise for perspectives applications, such as the photocatalytic generation of Hydrogen via the dissociation of water.

Acknowledgment:

The authors would like to thank the departmental council of La Manche (CD50) for the financial support of this work carried out within the LUSAC laboratory (I. ZAHWA).

References

[1] R. Dholam, N. Patel, M. Adami, A. Miotello, Physically and chemically synthesized TiO2 composite thin films for hydrogen production by photocatalytic water splitting, Int. J. Hydrogen Energy. 33 (2008) 6896–6903. https://doi.org/10.1016/j.ijhydene.2008.08.061.

[2] M. Ni, M.K.H.L. Ã, D.Y.C. Leung, K. Sumathy, A review and recent developments in photocatalytic water-splitting using TiO 2 for hydrogen production, 11 (2007) 401–425. https://doi.org/10.1016/j.rser.2005.01.009.

[3] X. Chen, S.S. Mao, Titanium dioxide nanomaterials: Synthesis, properties, modifications and applications, Chem. Rev. 107 (2007) 2891–2959. https://doi.org/10.1021/cr0500535.

[4] C.H. Liao, C.W. Huang, J.C.S. Wu, Hydrogen production from semiconductor-based photocatalysis via water splitting, Catalysts. 2 (2012) 490–516. https://doi.org/10.3390/catal2040490.

[5] M.V. Dozzi, C. D'Andrea, B. Ohtani, G. Valentini, E. Selli, Fluorine-doped TiO2 materials: Photocatalytic activity vs time-resolved photoluminescence, J. Phys. Chem. C. 117 (2013) 25586–25595. https://doi.org/10.1021/jp4095563.

[6] J. Liqiang, Q. Yichun, W. Baiqi, L. Shudan, J. Baojiang, Y. Libin, F. Wei, F. Honggang, S. Jiazhong, Review of photoluminescence performance of nano-sized semiconductor materials and its relationships with photocatalytic activity, Sol. Energy Mater. Sol. Cells. 90 (2006) 1773–1787. https://doi.org/10.1016/j.solmat.2005.11.007.

[7] C.M. Malengreaux, S.L. Pirard, G. Léonard, J.G. Mahy, M. Herlitschke, B. Klobes, R. Hermann, B. Heinrichs, J.R. Bartlett, Study of the photocatalytic activity of Fe3+, Cr3+, La3+and Eu3+single-doped and co-doped TiO2catalysts produced by aqueous sol-gel processing, J. Alloys Compd. 691 (2017) 726–738. https://doi.org/10.1016/j.jallcom.2016.08.211.

[8] M. Szkoda, K. Siuzdak, A. Lisowska-Oleksiak, Non-metal doped TiO2 nanotube arrays for high efficiency photocatalytic decomposition of organic species in water, Phys. E Low-Dimensional Syst. Nanostructures. 84 (2016) 141–145. https://doi.org/10.1016/j.physe.2016.06.004.

[9] J.C. Tristão, F. Magalhães, P. Corio, M.T.C. Sansiviero, Electronic characterization and photocatalytic properties of CdS/TiO2 semiconductor composite, J. Photochem. Photobiol. A Chem. 181 (2006) 152–157. https://doi.org/10.1016/j.jphotochem.2005.11.018.

[10] S.A.K. Leghari, S. Sajjad, F. Chen, J. Zhang, WO3/TiO2 composite with morphology change via hydrothermal template-free route as an efficient visible light photocatalyst, Chem. Eng. J. 166 (2011) 906–915. https://doi.org/10.1016/j.cej.2010.11.065.

[11] T. Teka, Current State Of Doped-Tio 2 Photocatalysts And Synthesis Methods To Prepare Tio 2 Films : A Re- view, Int. J. Technol. Enhanc. Emerg. Eng. Res. 3 (2015) 14–18.

[12] Z. Zhao, X. Zhao, J. Yi, Q. Liu, Effects of nonmetal doping on electronic structures and optical property

of anatase TiO2 from first-principles calculations, Xiyou Jinshu Cailiao Yu Gongcheng/Rare Met. Mater. Eng. 44 (2015) 1568–1574. https://doi.org/10.1016/s1875-5372(15)30094-1.
[13] M. Umadevi, M. Sangari, R. Parimaladevi, A. Sivanantham, J. Mayandi, Enhanced photocatalytic, antimicrobial activity and photovoltaic characteristics of fluorine doped TiO2 synthesized under ultrasound irradiation, J. Fluor. Chem. 156 (2013) 209–213. https://doi.org/10.1016/j.jfluchem.2013.10.011.
[14] D.H. Lee, B. Swain, D. Shin, N.K. Ahn, J.R. Park, K.S. Park, One-pot wet chemical synthesis of fluorine-containing TiO2 nanoparticles with enhanced photocatalytic activity, Mater. Res. Bull. 109 (2019) 227–232. https://doi.org/10.1016/j.materresbull.2018.09.027.
[15] H. Sun, S. Wang, H.M. Ang, M.O. Tadé, Q. Li, Halogen element modified titanium dioxide for visible light photocatalysis, Chem. Eng. J. 162 (2010) 437–447. https://doi.org/10.1016/j.cej.2010.05.069.
[16] J.C. Yu, J. Yu, W. Ho, Z. Jiang, L. Zhang, Effects of F- doping on the photocatalytic activity and microstructures of nanocrystalline TiO2 powders, Chem. Mater. 14 (2002) 3808–3816. https://doi.org/10.1021/cm020027c.
[17] D. Li, H. Haneda, S. Hishita, N. Ohashi, N.K. Labhsetwar, Fluorine-doped TiO 2 powders prepared by spray pyrolysis and their improved photocatalytic activity for decomposition of gas-phase acetaldehyde, J. Fluor. Chem. 126 (2005) 69–77. https://doi.org/10.1016/j.jfluchem.2004.10.044.
[18] V. Brezov, Phenol decomposition using M " + / TiO2 photocatalysts supported by the sol-gel technique on glass fibres, 20 (1997) 2–6.
[19] H. Jiang, H. Song, Z. Zhou, X. Liu, G.M. Ã, The roles of Li + and F À ions in Li – F-codoped TiO 2 system, 68 (2007) 1830–1835. https://doi.org/10.1016/j.jpcs.2007.01.027.
[20] H. Jiang, H. Song, Z. Zhou, X. Liu, G. Meng, Characterization of LiF-doped TiO2 and its photocatalytic activity for decomposition of trichloromethane, Mater. Res. Bull. 43 (2008) 3037–3046. https://doi.org/10.1016/j.materresbull.2007.11.009.
[21] T. Athar, Smart precursors for smart nanoparticles, in: Emerg. Nanotechnologies Manuf., Elsevier, 2015: pp. 444–538.
[22] O. Carp, C.L. Huisman, A. Reller, Photoinduced reactivity of titanium dioxide, Prog. Solid State Chem. 32 (2004) 33–177. https://doi.org/https://doi.org/10.1016/j.progsolidstchem.2004.08.001.
[23] M.S. Hegde, G. Madras, K.C. Patil, Noble Metal Ionic Catalysts, Acc. Chem. Res. 42 (2009) 704–712. https://doi.org/10.1021/ar800209s.
[24] F. Deganello, G. Marcì, G. Deganello, Citrate-nitrate auto-combustion synthesis of perovskite-type nanopowders: A systematic approach, J. Eur. Ceram. Soc. 29 (2009) 439–450. https://doi.org/10.1016/j.jeurceramsoc.2008.06.012.
[25] C.N.R. Rao, Chemical synthesis of solid inorganic materials, Mater. Sci. Eng. B. 18 (1993) 1–21. https://doi.org/10.1016/0921-5107(93)90109-Z.
[26] E. Chimie, THÈSE POUR OBTENIR LE GRADE DE DOCTEUR DE L ' UNIVERSITÉ DE MONTPELLIER Conversion des nitrates d ' actinides en oxydes par combustion en solution Présentée par Julien, (2019).
[27] F. Deganello, A.K. Tyagi, Solution combustion synthesis, energy and environment: Best parameters for better materials, Prog. Cryst. Growth Charact. Mater. 64 (2018) 23–61. https://doi.org/10.1016/j.pcrysgrow.2018.03.001.
[28] M. Mouyane, B. Jaber, B. Bendjemil, J. Bernard, D. Houivet, J.G. Noudem, Sintering behavior of magnesium aluminate spinel MgAl 2 O 4 synthesized by different methods, Int. J. Appl. Ceram. Technol. 16 (2019) 1138–1149. https://doi.org/10.1111/ijac.13172.
[29] M. Mouyane, B. Itaalit, J.Ô. Bernard, D. Houivet, J.G. Noudem, Flash combustion synthesis of electron doped-CaMnO3 thermoelectric oxides, Powder Technol. 264 (2014) 71–77. https://doi.org/10.1016/j.powtec.2014.05.022.
[30] R. V. Mangalaraja, J. Mouzon, P. Hedström, I. Kero, K.V.S. Ramam, C.P. Camurri, M. Odén, Combustion synthesis of Y2O3 and Yb-Y2O3. Part I. Nanopowders and their characterization, J. Mater. Process. Technol. 208 (2008) 415–422. https://doi.org/10.1016/j.jmatprotec.2008.01.023.
[31] Y. Wang, L. Gong, Y. Li, Z. Wei, Combustion synthesis of La0.8Sr0.2MnO3 and its effect on HMX thermal decomposition, Chinese J. Chem. Eng. 18 (2010) 397–401. https://doi.org/10.1016/S1004-9541(10)60237-6.
[32] D.A. Fumo, J.R. Jurado, A.M. Segadães, J.R. Frade, Combustion synthesis of iron-substituted strontium titanate perovskites, Mater. Res. Bull. 32 (1997) 1459–1470. https://doi.org/10.1016/S0025-5408(97)00117-7.
[33] G. Avgouropoulos, T. Ioannides, Selective CO oxidation over CuO-CeO2 catalysts prepared via the urea-nitrate combustion method, Appl. Catal. A Gen. 244 (2003) 155–167. https://doi.org/10.1016/S0926-860X(02)00558-6.
[34] R.K. Selvan, C.O. Augustin, L.J. Berchmans, R. Saraswathi, Combustion synthesis of CuFe2O4, Mater.

Res. Bull. 38 (2003) 41–54. https://doi.org/10.1016/S0025-5408(02)01004-8.
[35] S. Yin, D. Chen, W. Tang, Combustion synthesis and luminescent properties of CaTiO3: Pr, Al persistent phosphors, J. Alloys Compd. 441 (2007) 327–331. https://doi.org/10.1016/j.jallcom.2006.09.120.
[36] P. Naderi, S.M. Masoudpanah, S. Alamolhoda, Magnetic properties of Li0.5Fe2.5O4 nanoparticles synthesized by solution combustion method, Appl. Phys. A Mater. Sci. Process. 123 (2017) 1–8. https://doi.org/10.1007/s00339-017-1304-8.
[37] N.P. Bansal, Low temperature synthesis of CaO-SiO2 glasses having stable liquid-liquid immiscibility by the sol-gel process, J. Mater. Sci. 27 (1992) 2922–2933. https://doi.org/10.1007/BF01154101.
[38] R.A. Spurr, H. Myers, Quantitative Analysis of Anatase-Rutile Mixtures with an X-Ray Diffractometer, Anal. Chem. 29 (1957) 760–762. https://doi.org/10.1021/ac60125a006.
[39] S. Challagulla, S. Roy, The role of fuel to oxidizer ratio in solution combustion synthesis of TiO2and its influence on photocatalysis, J. Mater. Res. 32 (2017) 2764–2772. https://doi.org/10.1557/jmr.2017.244.
[40] L.E. Oi, M.Y. Choo, H.V. Lee, H.C. Ong, S.B.A. Hamid, J.C. Juan, Recent advances of titanium dioxide (TiO2) for green organic synthesis, RSC Adv. 6 (2016) 108741–108754. https://doi.org/10.1039/c6ra22894a.
[41] D.A.H. Hanaor, C.C. Sorrell, Review of the anatase to rutile phase transformation, J. Mater. Sci. 46 (2011) 855–874. https://doi.org/10.1007/s10853-010-5113-0.
[42] J. Yang, J.M.F. Ferreira, Inhibitory effect of the Al2O3-SiO2 mixed additives on the anatase-rutile phase transformation, Mater. Lett. 36 (1998) 320–324. https://doi.org/10.1016/S0167-577X(98)00042-1.
[43] G. Rothenberger, J. Moser, M. Gratzel, N. Serpone, D.K. Sharma, Charge carrier trapping and recombination dynamics in small semiconductor particles, J. Am. Chem. Soc. 107 (1985) 8054–8059. https://doi.org/10.1021/ja00312a043.
[44] J. Navas, A. Sánchez-Coronilla, T. Aguilar, M. Desireé, N.C. Hernández, R. Alcántara, C. Fernández-Lorenzo, J. Martín-Calleja, Thermo-selective Tm x Ti 1− x O 2− x/2 nanoparticles: from Tm-doped anatase TiO 2 to a rutile/pyrochlore Tm 2 Ti 2 O 7 mixture. An experimental and theoretical study with a photocatalytic application, Nanoscale. 6 (2014) 12740–12757.
[45] K. Rajeshwar, Photoelectrochemistry and the environment, J. Appl. Electrochem. 25 (1995) 1067–1082.
[46] S. Livraghi, M. Chiesa, M.C. Paganini, E. Giamello, On the Nature of Reduced States in Titanium Dioxide As Monitored by Electron Paramagnetic Resonance. I: The Anatase Case, J. Phys. Chem. C. 115 (2011) 25413–25421. https://doi.org/10.1021/jp209075m.
[47] S. Livraghi, S. Maurelli, M.C. Paganini, M. Chiesa, E. Giamello, Probing the local environment of Ti3+ ions in TiO2 (rutile) by 17O HYSCORE, Angew. Chemie - Int. Ed. 50 (2011) 8038–8040. https://doi.org/10.1002/anie.201100531.
[48] M. Chiesa, M.C. Paganini, S. Livraghi, E. Giamello, Charge trapping in TiO2 polymorphs as seen by Electron Paramagnetic Resonance spectroscopy, Phys. Chem. Chem. Phys. 15 (2013) 9435–9447. https://doi.org/10.1039/c3cp50658d.
[49] E. Serwicka, M.W. Schlierkamp, R.N. Schindler, No Title, Zeitschrift Für Naturforsch. A. 36 (1981) 226–232. https://doi.org/doi:10.1515/zna-1981-0305.
[50] E.G. Panarelli, S. Livraghi, S. Maurelli, V. Polliotto, M. Chiesa, E. Giamello, Role of surface water molecules in stabilizing trapped hole centres in titanium dioxide (anatase) as monitored by electron paramagnetic resonance, J. Photochem. Photobiol. A Chem. 322–323 (2016) 27–34. https://doi.org/10.1016/j.jphotochem.2016.02.015.
[51] S. Pal, A.M. Laera, A. Licciulli, M. Catalano, A. Taurino, Biphase TiO2 microspheres with enhanced photocatalytic activity, Ind. Eng. Chem. Res. 53 (2014) 7931–7938. https://doi.org/10.1021/ie404123f.
[52] R.J. Tayade, P.K. Surolia, R.G. Kulkarni, R. V Jasra, Photocatalytic degradation of dyes and organic contaminants in water using nanocrystalline anatase and rutile TiO2, Sci. Technol. Adv. Mater. 8 (2007) 455.
[53] D. Li, N. Ohashi, S. Hishita, T. Kolodiazhnyi, H. Haneda, Origin of visible-light-driven photocatalysis: A comparative study on N/F-doped and N-F-codoped TiO2 powders by means of experimental characterizations and theoretical calculations, J. Solid State Chem. 178 (2005) 3293–3302. https://doi.org/10.1016/j.jssc.2005.08.008.
[54] S. Liu, J. Yu, B. Cheng, M. Jaroniec, Fluorinated semiconductor photocatalysts: Tunable synthesis and unique properties, Adv. Colloid Interface Sci. 173 (2012) 35–53. https://doi.org/10.1016/j.cis.2012.02.004.
[55] J.S. Park, W. Choi, Enhanced remote photocatalytic oxidation on surface-fluorinated TiO2, Langmuir. 20 (2004) 11523–11527.
[56] D.C. Hurum, A.G. Agrios, K.A. Gray, T. Rajh, M.C. Thurnauer, Explaining the enhanced photocatalytic activity of Degussa P25 mixed-phase TiO2 using EPR, J. Phys. Chem. B. 107 (2003) 4545–4549. https://doi.org/10.1021/jp0273934.

Table of figures

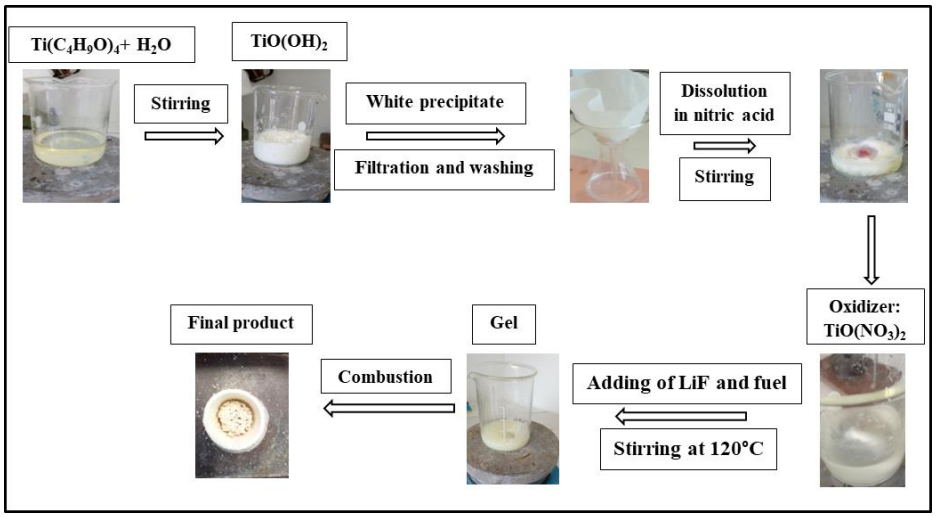

Fig. 1. Sequential steps of the synthesis for flash combustion of the TiO_2 + (*x* LiF) powders using glycine or urea.

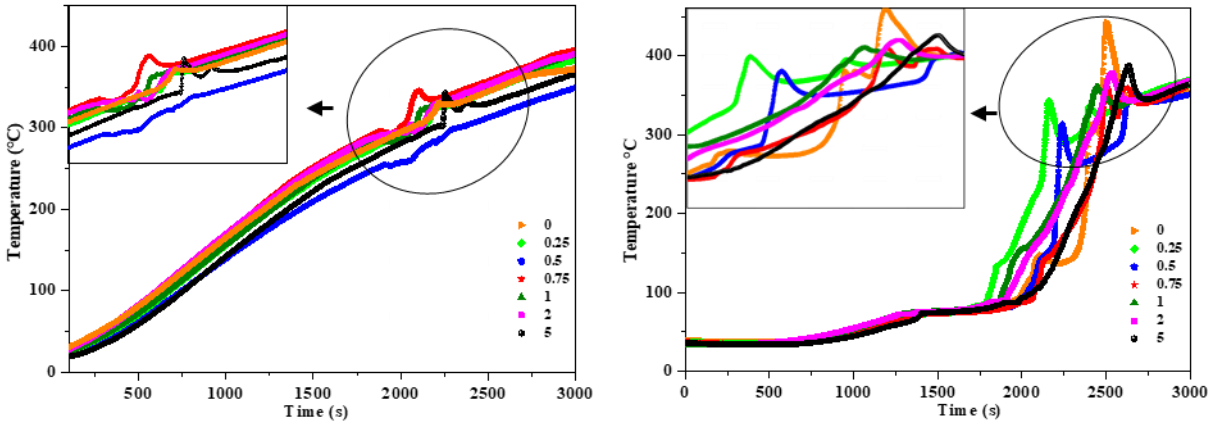

Fig. 2. Temperature-time curves measured at the crucible level in the furnace during the flash combustion reactions of the TiO_2 + (*x* LiF) powders. (a) glycine, (b) urea.

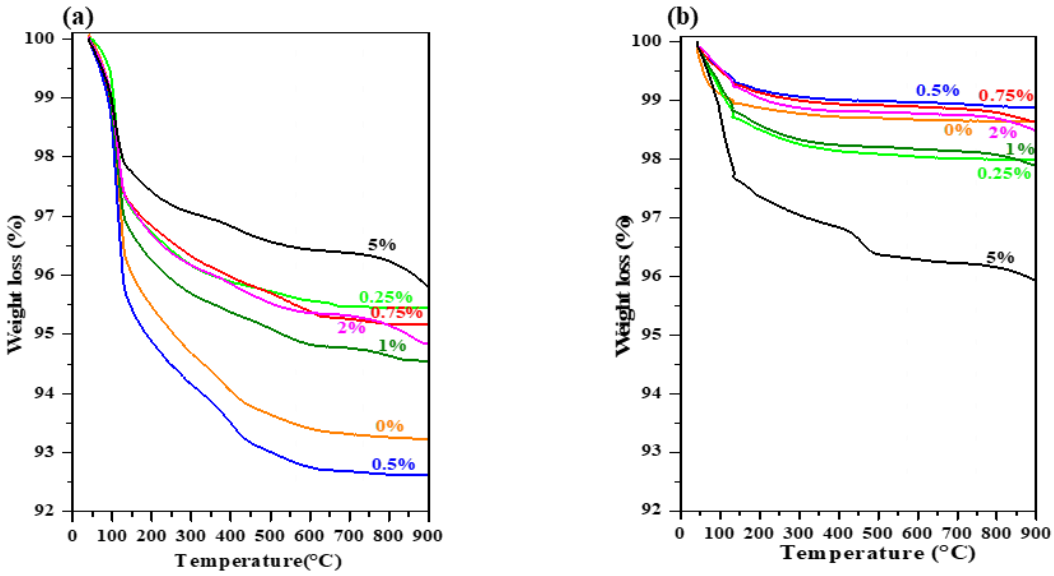

Fig. 3. TG curves of TiO_2 + (*x* LiF) as-synthesized powders. (a) glycine, (b) urea.

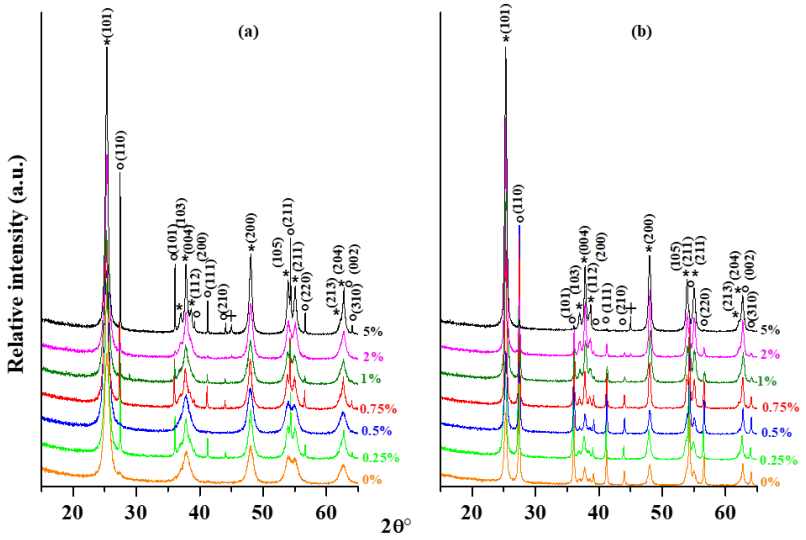

Fig. 4. X-ray diffraction patterns of the TiO_2 + (*x* LiF) as-synthesized powders (a) made by glycine, (b) made by urea. *anatase, °rutile, +LiF.

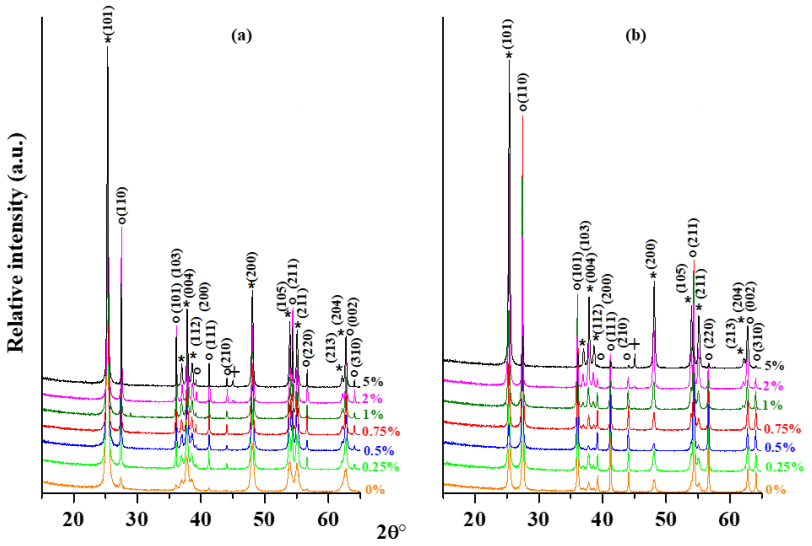

Fig. 5. X-ray diffraction patterns of the powders heat treated at 500 °C (a) made by glycine, (b) made by urea. *anatase, ° rutile, +LiF.

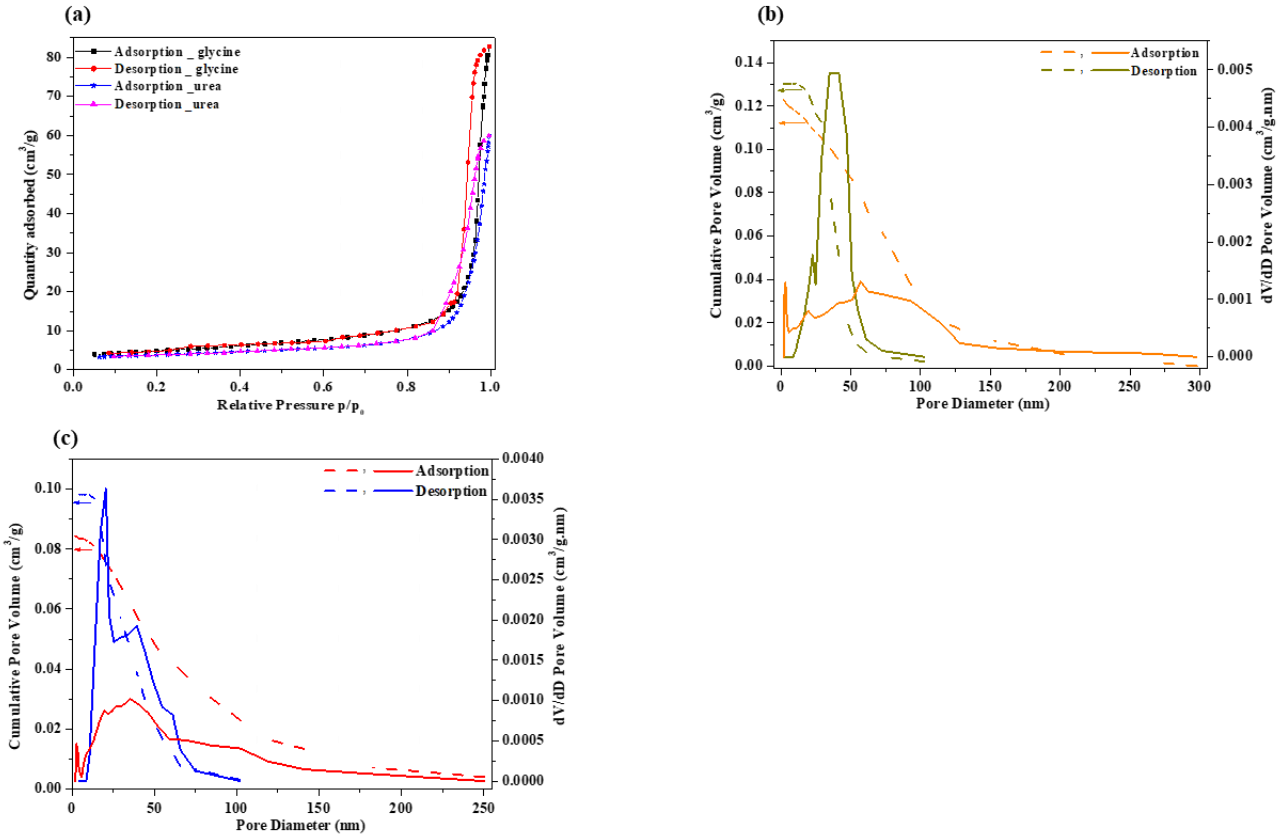

Fig. 6. (a) Nitrogen adsorption-desorption isotherms of the sample TiO_2+2 wt. %LiF, heat treated at 500 °C, made by glycine and urea. (b and c) The pore size distribution curve of these two samples made by glycine and urea respectively.

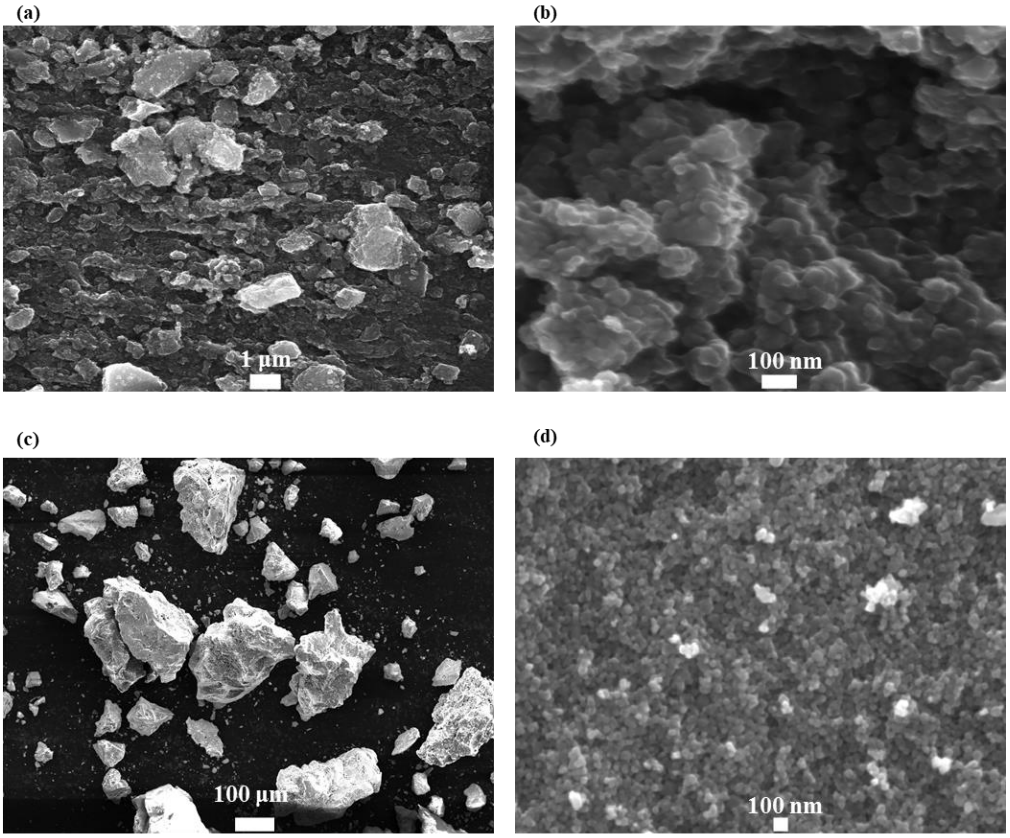

Fig. 7. SEM micrographs of the nanopowders TiO_2+2 wt. %LiF synthesized by F.C., annealed at 500 ºC: (a, b) made by glycine, (c, d) made by urea.

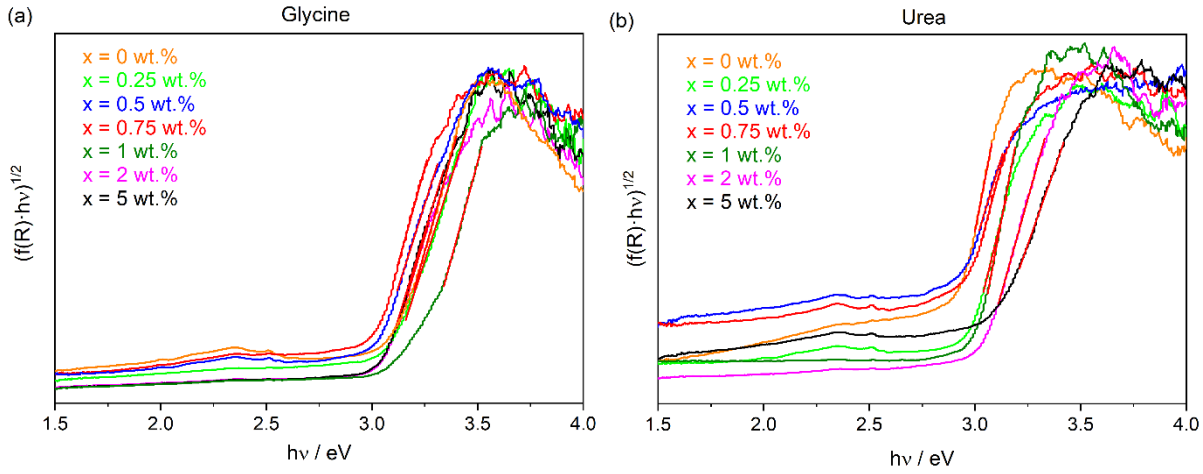

Fig. 8. Tauc plot TiO_2 +(*x* LiF) samples prepared using glycine (a) and urea (b), heat treated at 500 °C.

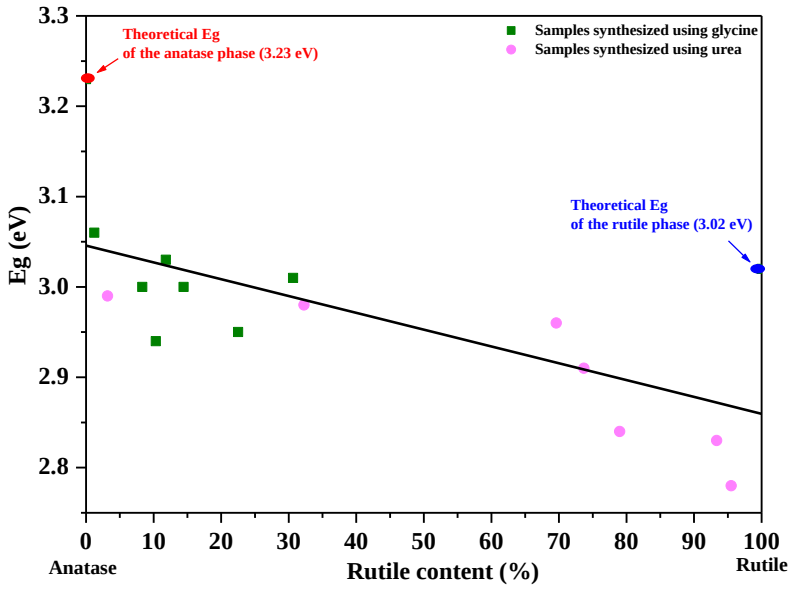

Fig. 9. Band gap (Eg) variation as a function of the rutile content (%) of the samples TiO_2 + (*x* LiF) prepared using glycine and urea.

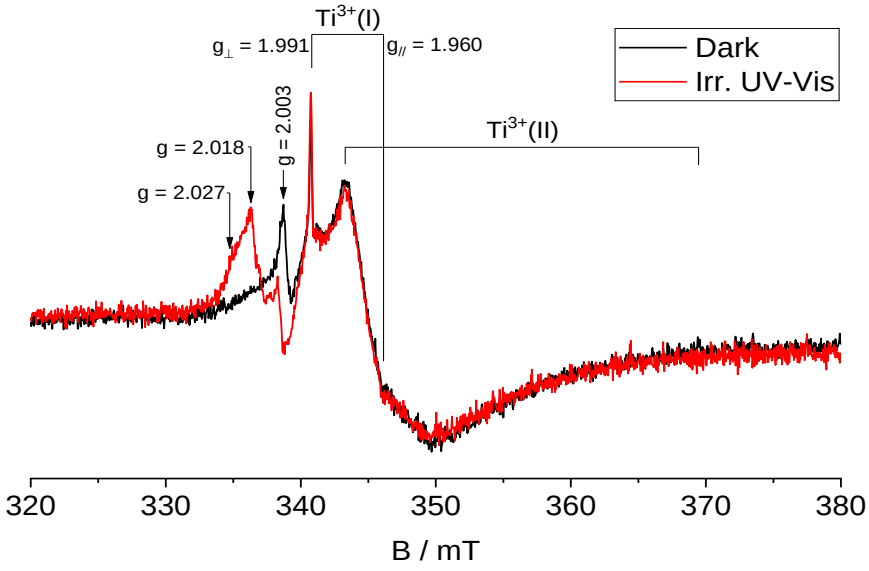

Fig. 10. Comparison of the EPR spectrum recorder at 77K in dark with the same spectrum obtained under UV-vis light irradiation of the sample TiO_2+2 wt. %LiF, heat treated at 500 °C made by glycine.

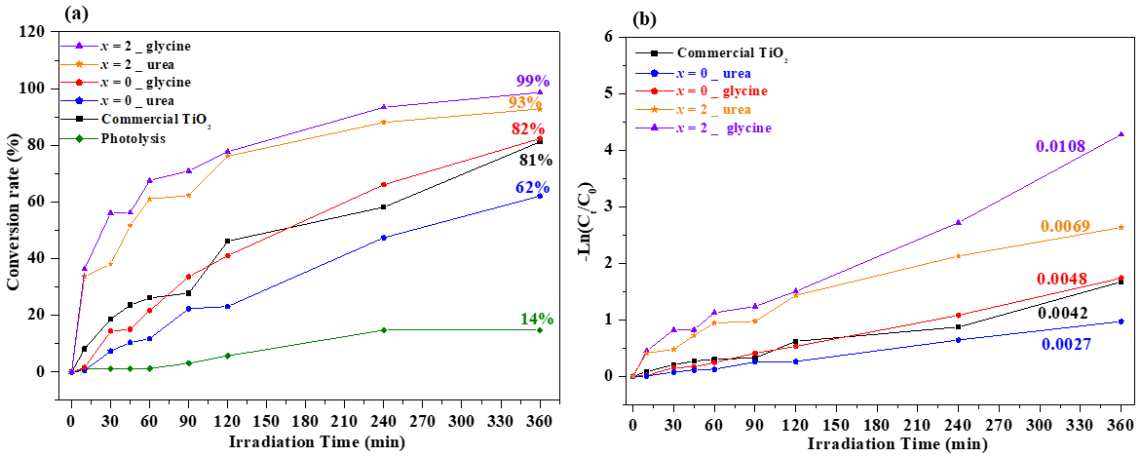

Fig. 11. (a) Photocatalytic degradation of MB under UV-visible irradiation using the different samples TiO_2 + (*x* LiF) _Fuel. (b) Photodegradation kinetics of MB in the presence of the different samples. Apparent reaction rate constants (K) of the samples are mentioned in the **fig.11b**.